BULLETIN OF THE POLISH ACADEMY OF SCIENCES
TECHNICAL SCIENCES, Vol. 74(2), 2026, Article number: e157064
DOI: 10.24425/bpasts.2025.157064

Thermo-optical, structural, and morphological characterization of ZnO:PQX composite thin films

Natalia NOSIDLAK[1]*, Katarzyna WOJTASIK[1], Piotr DULIAN[2], Patryk SZYMCZAK[3], and Mateusz PIZ[4]

[1] Department of Physics, Faculty of Materials Engineering and Physics, Cracow University of Technology, ul. Podchorążych 1, 30-084 Kraków, Poland
[2] Faculty of Chemical Engineering and Technology, Cracow University of Technology, ul. Warszawska 24, 31-155 Kraków, Poland
[3] Faculty of Materials Science and Ceramics, AGH University of Science and Technology, al. Mickiewicza 30, 30-059 Kraków, Poland
[4] Department of Inorganic and Analytical Chemistry, Faculty of Chemical Engineering and Technology, West Pomeranian University of Technology in Szczecin, al. Piastów 42, 71-065 Szczecin, Poland

Abstract. This work presents a detailed study of thin zinc oxide (ZnO) films and ZnO composite films doped with the organic luminescent dye PQX, prepared by the sol-gel method and spin coating. The optical, thermo-optical, structural, and morphological properties of these films were investigated using spectroscopic ellipsometry, X-ray diffraction, thermal analysis, atomic force microscopy, and scanning electron microscopy. The PQX dye showed strong absorption in the blue region of the spectrum with a large Stokes shift, indicating potential for luminescent solar concentrator (LSC) applications. Thermal studies revealed limited stability of PQX in thin films with partial degradation beginning at 100°C and complete decomposition above 300°C, which affected the optical and structural properties of the composite films. Annealing led to an amorphous state transition of the organic component and increased porosity in the ZnO matrix. ZnO:PQX films exhibited increased surface roughness and reduced refractive index compared to pure ZnO. These findings suggest that while PQX enhances certain optical properties, its thermal instability limits the performance of ZnO:PQX composites in LSC devices, highlighting the need for further materials optimization.

Keywords: ellipsometry; ZnO thin films; organic dye; sol-gel.

1. INTRODUCTION

Zinc oxide (ZnO) is widely regarded as one of the most promising materials employed in electronics, optoelectronics, and renewable energy technologies. Thin ZnO films are characterized by high optical transmittance and excellent semiconductor properties such as the wide band gap ($E_g^{\text{bulk}} = 3.37$ eV), a high exciton binding energy (~ 60 meV at room temperature), and resistance to environmental factors [1]. ZnO, in the form of thin films, is used not only in solar cells and light-emitting diodes but also in sensors [2], protective coatings, and innovative light concentrators such as luminescent solar concentrators (LSCs) [1, 3]. The rapid development of synthesis methods and the ability to modify the ZnO structure position it as a pioneering material in designing efficient and durable future devices.

LSCs are highly efficient solar radiation concentrators that exhibit minimal sensitivity to lighting conditions. They consist of a waveguide matrix with luminescent components dispersed within it, which absorb radiation and emit it in a different spectral range suitable for the attached solar cell.

Previously, literature reported ZnO as luminescent centers in LSC designs. For example, Fimbres-Romero and Lopez-Delgado achieved promising results with transparent and colorless LSCs based on ZnO quantum dots embedded in polymethyl methacrylate (PMMA) polymer matrix [3]. Meanwhile, Ibrahim *et al.* studied the effect of adding ZnO nanoparticles on the optical properties and photovoltaic efficiency of the organic dye Rhodamine C, observing improved parameters with increasing addition of ZnO nanoparticles [4].

To develop new solutions for the matrix in LSC devices, researchers are turning to thin sol-gel coatings based on the composition used to produce ZnO layers. These coatings showed no luminescence quenching effect when doped with organic materials [4–6]. One of the key factors influencing the luminescence efficiency of ZnO films is the surface morphology [7]. Layers with well-controlled grain structure and smooth surfaces enhance photon absorption and reduce defects, which can act as nonradiative recombination centers, leading to improved luminescence. The addition of organic luminophores to thin ZnO layers can further improve emission properties and light conversion efficiency [4].

Materials intended for use in LSCs should also demonstrate high thermal stability. Recent literature emphasizes significant interest in this aspect. Guo *et al.* described a perovskite-PMMA composite with high thermal (up to 160°C) and environmental stability [8]. Similarly, Hong *et al.* investigated the thermal and UV photostability of inorganic-polymer composites based on PDMS (polydimethylsiloxane), achieving excellent results [9]. Thin ZnO films also demonstrate good thermal stability [10–12], making them suitable for use in LSCs. For example, Dalouji

*e-mail: natalia.nosidlak@pk.edu.pl

Manuscript submitted 2025-09-16, revised 2025-11-30, initially accepted for publication 2026-01-11, published in March 2026.

studied the effect of annealing on the optical properties and thermal stability of thin ZnO films. The results indicate that high-temperature annealing (400–600°C) can improve the ordering of the layer structure, reduce defects, and modify internal interactions within the material, thereby enhancing thermal stability [12].

In our previous work [13], which examined the effect of temperature on the optical constants of thin ZnO and Al-doped ZnO films, we demonstrated high thermal stability and discussed the relationship between their structure and optical properties. The inclusion of organic materials may also influence the thermal stability of composite layers.

In this work, we present the results of optical, thermo-optical, X-ray diffraction, and surface morphology studies of thin ZnO films and composite ZnO films doped with the luminescent dye 6-*N,N*-diphenylamino-3-phenyl-1-methyl-1*H*-pyrazolo[3,4-*b*]quinoxaline (PQX) – ZnO:PQX, prepared via the sol-gel method and applied by spin coating. Surface morphology was examined using scanning electron microscopy (SEM) and atomic force microscopy (AFM). Thickness, refractive index, and thermo-optical properties were investigated using spectroscopic ellipsometry.

2. MATERIAL DESCRIPTIONS AND RESEARCH METHODOLOGY

There are many techniques for producing thin oxide films. The ZnO and ZnO:PQX thin films were fabricated using the sol-gel method, which enables precise control over the synthesis parameters. The process involved preparing solutions containing precursors of the respective metals, applying the sol onto the substrate surface using the spin-coating technique, and a calcination step under controlled conditions (150°C for 1 h). The composition of the sol used to create the reference ZnO layer (base sol) included: zinc acetate, ethanol, water, diethanolamine (DEA), and surfactant dihydro-3-(tetrapropenyl)furan-2,5-dione (TPSA). The components were mixed in a ratio of 1:28.5:2:0.5:1.7, respectively. The sol synthesis was carried out for 2.5 h at 50°C. The composite ZnO:PQX film was made from a sol with the composition of the base sol, with the addition of PQX dye (0.25%). The dye was added in the form of an ethanolic solution to the base sol. The layers were prepared after 24 h by the spin-coating method (2000 rpm, 30 s) on silicon and soda-lime glass substrates. The structures were heated at 150°C for 1 h. PQX, synthesized according to the procedure described previously in [14], was used as an organic dye. Figure 1 shows the synthesis scheme of the PQX system.

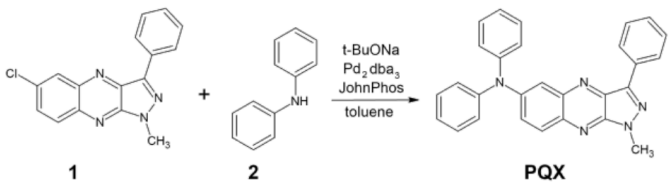

Fig. 1. PQX system synthesis diagram

The compound 6-chloro-1-methyl-3-phenyl-1*H*-pyrazolo-[3,4-*b*]quinoxaline **1**, which was the starting substrate in the synthesis of PQX dye, was obtained by a two-step regiospecific synthesis described previously in [15] with yields of 72% and 54% in the individual steps, respectively. The PQX dye was prepared by palladium – catalyzed aminoarylation of pyrazoloquinoxaline derivative **1** with diphenylamine **2**. In this reaction **1** (188 mg, 0.64 mmol), diphenylamine **2** (130 mg, 0.77 mmol), sodium tert-butoxide (86 mg, 0.90 mmol), Pd_2dba_3 (tris-(dibenzylideneacetone)dipalladium(0), 5.9 mg, 0.0064 mmol, 1 mol%), JohnPhos (2-(di-tert-butylphosphino)biphenyl, 3.8 mg, 0.0128 mmol, 2 mol%), and toluene (2 mL) were placed in a Schlenk flask. The reagents were purged with argon. The reaction was allowed to proceed under argon at 80°C for 48 h. After cooling, the reaction mixture was filtered and purified by column chromatography on alumina with toluene as eluent. The PQX product was crystallized from petroleum ether 60/90. PQX was ultimately obtained in a 53% yield. The obtained product was characterized by recording nuclear magnetic resonance spectra (^{1}H and ^{13}C NMR) on Bruker Avance III 600, and elemental analysis was conducted at Elementar Vario MICRO cube.

6-*N,N*-diphenylamino-1-methyl-3-phenyl-1*H*-pyrazolo[3,4-*b*]quinoxaline (PQX):

bright red crystals, 143 mg, 53% yield, ^{1}H NMR ($CDCl_3$, 600 MHz): δ(ppm) 8.55 (dd, J = 7.8, 0.6 Hz, 2H), 7.95 (d, J = 9.6 Hz, 1H), 7.73 (d, J = 2.4 Hz, 1H), 7.65 (dd, J = 9.0, 2.4 Hz, 1H), 7.50 (t, J = 7.8 Hz, 2H), 7.40 – 7.38 (m, 1H), 7.36 – 7.33 (m, 4H), 7.22 (d, J = 7.8 Hz, 4H), 7.16 – 7.14 (m, 2H), 4.26 (s, 3H); ^{13}C NMR ($CDCl_3$): δ(ppm) 147.3, 147.0, 143.0, 142.8, 141.3, 138.6, 135.3, 131.9, 129.6, 129.1, 128.71, 128.67, 128.5, 126.7, 125.4, 124.2, 118.2, 34.3. Anal. Calcd for $C_{28}H_{21}N_5$: C, 78.69; H, 4.92; N, 16.39. Found: C, 78.67; H, 4.75; N, 16.55.

The measurement of absorption spectra was performed using a double-beam spectrophotometer, Perkin Elmer model Lambda 900, with a measurement range from 200 to 2500 nm. Photoluminescence spectra were recorded using an HR4000CG-UVNIR spectrometer from Ocean Optics. The organic compound PQX in solution form was excited using a Spectroline UV lamp with a wavelength of 365 nm.

X-ray diffraction (XRD) analysis of the samples was conducted using a Rigaku SmartLab SE powder X-ray diffractometer. The instrument was equipped with a Hypix 400 semiconductor detector from the same manufacturer. Measurement conditions: Radiation source: Cu LFF (Long Fine Focus) anode tube, source power: 2.2 kW, measurement range: 10°–90°(2θ), slit width: 0.5°. Measurements were performed in continuous mode with a scanning speed of 2°/min. Phase identification was carried out using SmartLab Studio II software integrated with the ICDD PDF-4 database. Calibration of the diffraction system was performed using a standard silicon sample (NIST SRM 640c).

Differential thermal analysis (DTA) was performed using a Discovery SDT 650 (TA Instruments, USA) in an air atmosphere. The sample was heated at a rate of 10°/min over a temperature range of 20–500°C. During the measurement, heat

flow and mass loss were recorded simultaneously. The mass of the sample at the beginning of the measurement was 30 mg. The tests were conducted in corundum crucibles.

The optical and thermo-optical properties of the ZnO and ZnO:PQX thin films were characterized by spectroscopic ellipsometry. Measurements were conducted using a J.A. Woollam M-2000 ellipsometer, covering a spectral range of 193 to 1690 nm. The instrument was additionally equipped with a heating cell, enabling the investigation of changes in the optical properties of the samples within a temperature range from room temperature to 300°C.

Ellipsometry, a noncontact and nondestructive measurement technique, records the ellipsometric angles Ψ and Δ, as well as the depolarization of light reflected from the sample as a function of wavelength. By applying an appropriate optical model, the dispersion relations of the optical constants, film thickness, and energy gap of the studied layers were determined.

During measurement, changes in the polarization state of the reflected light were recorded. The ellipsometric angle Ψ corresponds to the change in the amplitude of polarized light upon reflection, while Δ corresponds to the phase difference between s- and p-polarized light before and after reflection [16,17]. These angles are related to the Fresnel reflection coefficients r_p and r_s through the fundamental ellipsometry equation (1) [18]:

$$\rho = \frac{r_p}{r_s} = \tan(\Psi)\exp(i\Delta), \tag{1}$$

where ρ represents the complex ratio of reflection coefficients, indicating the change in polarization of the reflected light.

A Bruker MultiMode 8 atomic force microscope (AFM) operating in tapping mode was employed to investigate the surface morphology and roughness of the deposited and annealed layers. Imaging was performed using RTESPA-300 probes, and surface roughness parameters, cross-sectional profiles, and 2D topographical micrographs were obtained using NanoScope Analysis 1.9 software.

SEM images were taken using a high-resolution scanning electron microscope Phenom XL by ThermoFisher Scientific with a CeB6 source, equipped with secondary electron (SED) and backscattered electron (BSE) detectors.

2.1. Thermo-optics

The temperature dependence of the optical constants, known as the thermo-optic effect, was investigated. Changes in the refractive index due to temperature variations can influence the operational lifespan and reliability of electronic devices and restrict their applicable conditions. According to Prod's-Homme theory [19], the variation of the refractive index n with temperature arises from changes in both the electronic polarizability and the material density. This relationship is expressed by equation (2):

$$\frac{dn}{dT} = \frac{\left(n^2-1\right)\left(n^2+2\right)}{6n}\left(\Phi-\beta\right), \tag{2}$$

where n is the refractive index, β denotes the volumetric thermal expansion coefficient, and Φ represents the temperature coefficient of electronic polarization, defined by equation (3) as:

$$\Phi = \frac{1}{P}\frac{dP}{dT}, \tag{3}$$

where P is the polarizability.

Equation (3) indicates that the refractive index increases with temperature when the electronic polarizability effect predominates.

Thermal processes, such as the evaporation of precursors or solvents, induce structural changes in the samples that directly affect both the refractive index and thickness of the thin films. The thermo-optic coefficient (TOC), defined as the temperature derivative of the refractive index at constant pressure, quantifies this effect in the following equation:

$$TOC = \frac{dn}{dT}. \tag{4}$$

Additionally, the thermal expansion coefficient (TEC), describing the change in sample thickness due to temperature variations, was calculated using equation (5):

$$TEC = \frac{d(thickness)}{dT}. \tag{5}$$

Notably, the refractive index exhibits an increase with temperature when electronic polarization dominates; conversely, the TOC becomes negative when thermal expansion effects prevail.

3. RESULTS AND DISCUSSION

Organic compounds used in LSCs should absorb radiation and re-emit it at a different wavelength suitable for the attached solar cell. A larger Stokes shift in LSC compounds enables more effective utilization of the absorbed light, which is crucial for achieving high energy efficiency of LSCs. Absorption and photoluminescence spectra for the compound PQX were recorded in several organic solvents (acetonitrile – ACN, tetrahydrofuran – THF, cyclohexane – CHX) and are presented in Fig. 2 and Fig. 3, respectively.

The absorption spectrum covers the UV and VIS range up to approximately 570 nm, with the main maximum at approximately 500 nm. Solvent polarity does not affect the position of

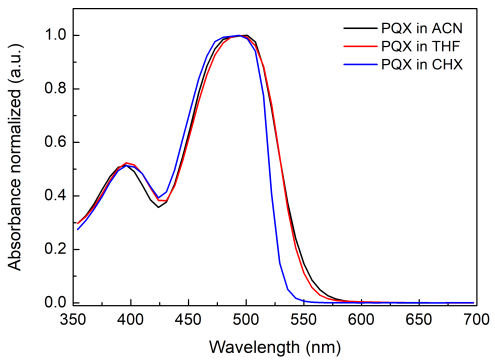

Fig. 2. Normalized absorption spectra of the PQX dye dissolved in various organic solvents: acetonitrile (ACN), tetrahydrofuran (THF), and cyclohexane (CHX)

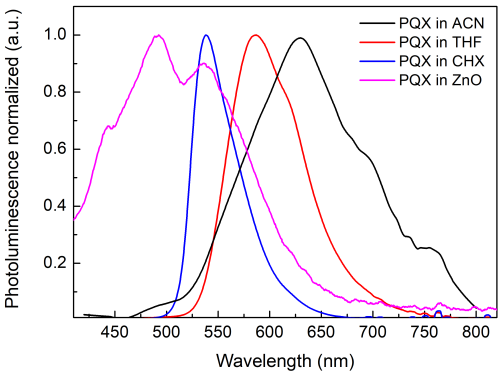

Fig. 3. Normalized photoluminescence spectra of the PQX dye dissolved in various organic solvents: acetonitrile (ACN), tetrahydrofuran (THF), cyclohexane (CHX), and a ZnO composite film

the absorption band maximum for the S0→S1 transitions of the tested dye, as previously observed for similar compounds [20]. The photoluminescence maximum occurs between 530 and 630 nm, depending on solvent polarity, as shown in Fig. 3 and in Table 1.

Table 1

Absorption and photoluminescence maxima, and the Stokes shift for the PQX dye in organic solvents

Parameter	Absorption maximum (nm)	Photoluminescence maximum (nm)	Stokes shift (nm)
ACN	501	629	128
THF	494	587	93
CHX	494	535	44

Figure 3 also presents the photoluminescence spectrum of a ZnO composite film containing 0.25 mol% PQX. Due to the low PQX content, the spectrum is dominated by the ZnO emission maximum, although the PQX contribution remains discernible. Organic compounds intended for use in LSCs should exhibit a large Stokes shift. The Stokes shift values for PQX reported in Table 1 (particularly in acetonitrile) indicate its potential suitability for LSC applications.

The optical model was fitted to the ellipsometric data using the CompleteEASE 5.15 software package. The PSemi-M0 parameterized semiconductor oscillator model was applied to determine the thickness and refractive index of the ZnO and ZnO:PQX thin films. The PSemi-M0 oscillator is derived from the Herzinger-Johs oscillator function [21]. Each PSemi-M0 oscillator consists of four polynomial spline functions connected end-to-end [22]. The model fulfils the Kramers-Kronig relations, and Gaussian oscillators are additionally incorporated into the optical model. This combination enhances the model flexibility, providing superior fitting to the experimental data by capturing both broad material effects and subtle spectral features that the Psemi-M0 model alone cannot adequately describe. All fitting parameters of the complete optical model for films deposited on silicon substrates are presented in Table 2. The fitting parameters of the Psemi-M0 oscillator are A (amplitude), B (broadening), E_0 (oscillator energy), PR, WR, AR, and O2R (polynomial control point parameters).

Figure 4 shows the dispersion relations of the ellipsometric angles Ψ and Δ for the ZnO:PQX film, along with the fitted model for the sample heated at 150°C. The model provides an excellent fit to the measurement data.

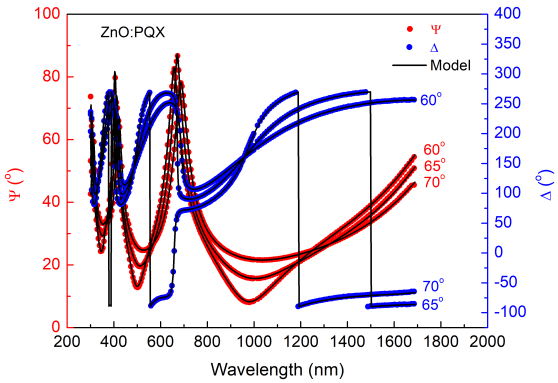

Fig. 4. The dispersion relations of the ellipsometric angles Ψ and Δ for the ZnO:PQX thin film on silicon (150°C 1 h), along with the fitted model

Table 2

Parameters of oscillator models fitted to ZnO and ZnO:PQX thin films at 150°C deposited on silicon

Sample	Oscillator type	E_0	A	B	WR	PR	AR	O2R
ZnO	Psemi-M0	1.810	0.116	0.182	2.408	0.220	0.234	0.040
	Gaussian	0.666	0.303	1.476	–	–	–	–
	Gaussian	3.850	0.075	0.826	–	–	–	–
	Gaussian	4.735	1.546	0.228	–	–	–	–
ZnO:PQX	Psemi-M0	1.721	0.196	0.244	3.365	0.441	0.390	0.050
	Gaussian	0.416	0.437	1.687	–	–	–	–
	Gaussian	3.489	0.030	0.373	–	–	–	–
	Gaussian	4.418	0.951	1.162	–	–	–	–

Based on the fitted optical model, the thicknesses and refractive indices of the studied layers were determined and are presented in Table 3.

Table 3
Thermo-optical parameters, thicknesses and root mean square roughness for ZnO and ZnO:PQX films on silicon

Parameter	ZnO	ZnO:PQX
Thickness (nm) at 150°C	396	536
n@300 nm	1.395	1.210
n@ 550 nm	1.368	1.216
TOC@300 nm (10^{-4}/°C)	–1.85	–1.49
TOC@550 nm (10^{-4}/°C)	–1.60	=-1.64
TEC (nm/°C)	0.019	0.063
σ_{RMS} (nm) (before heating)	2.3	37.1
σ_{RMS} (nm) (after heating)	0.4	28.6

The effect of temperature on optical parameters was investigated in two heating-cooling cycles in both samples: ZnO and ZnO:PQX on silicon substrates. The temperature-induced changes in thickness are shown in Fig. 5a and 5b, while the temperature dependence of the refractive index is presented in Fig. 6a and 6b. The TEC coefficients were determined from the slope coefficients of the curves in Fig. 5, and the TOC coefficients were determined from those in Fig. 6. The TEC and TOC coefficients are presented in Table 3.

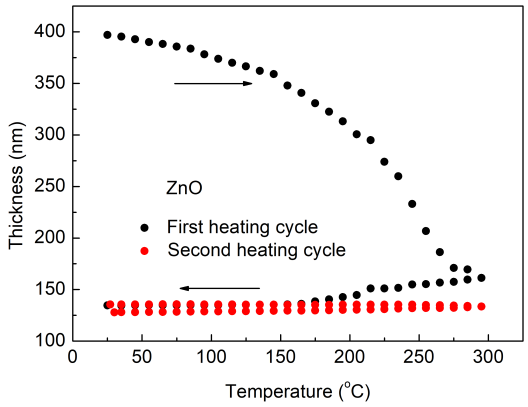

(a)

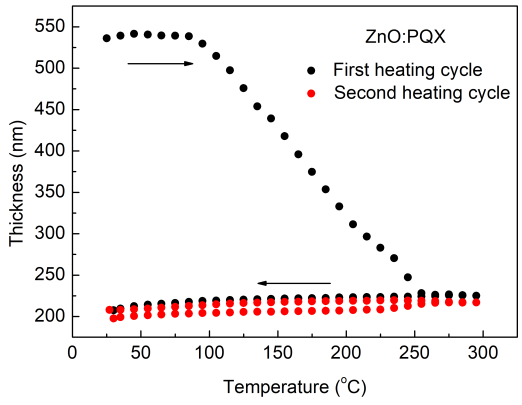

(b)

Fig. 5. Thermal hysteresis of the thickness of (a) ZnO and (b) ZnO:PQX thin films on silicon

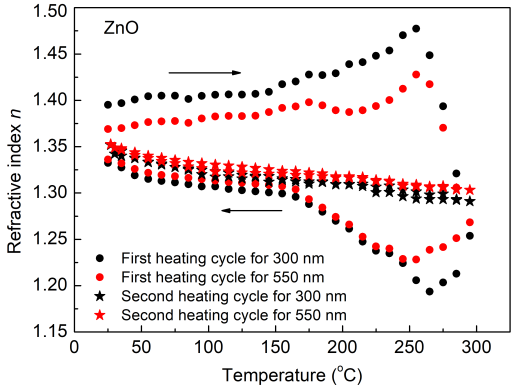

(a)

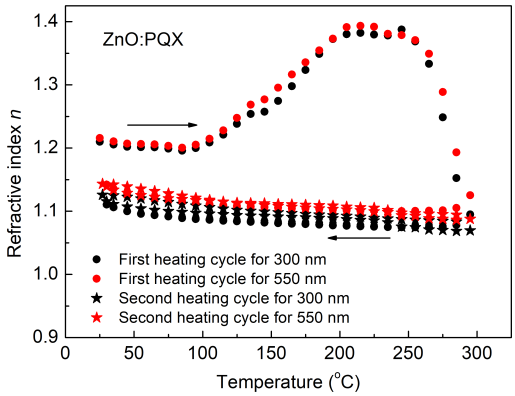

(b)

Fig. 6. Thermal hysteresis of the refractive index n of (a) ZnO, (b) ZnO:PQX thin films on silicon

In the first heating cycle, the thickness of the ZnO thin film gradually decreases with increasing temperature. For the ZnO:PQX composite film, a pronounced reduction in thickness occurs between 100°C and 250°C. Thermal analysis of PQX powder indicates rapid decomposition above 300°C, suggesting that some organic dye residues persist as stable components despite structural changes in thin films heated to 300°C. In Fig. 5b, distinct thermal effects around 100°C reflect processes such as organic ligand decomposition and porous structure reorganization, which reduce film thickness.

In the sol-gel method, organic additives like DEA and TPSA, which degrade during annealing, promote a highly porous structure. During cooling from 300°C in the first cycle, the ZnO film shows a continued decrease in refractive index, indicating ongoing structural reorganization initiated by heating. This may involve further release of residual gases or changes in surface morphology not completed during heating. In contrast, the ZnO:PQX film exhibits greater stability during cooling, suggesting that PQX modifies the structural dynamics.

After annealing the ZnO:PQX film at 300°C, the resulting structure consists of ZnO with PQX decomposition residues. These residues alter the optical and surface properties of the ZnO film, as evidenced by its modified refractive index compared to pure ZnO.

In the second heating cycle, changes in thickness and refractive index are less pronounced, and both films demonstrate improved thermal stability. At the end of the second cycle, refractive index values are lower than typical literature values for ZnO films. These low values (below 1.35 for ZnO and around 1.1 for ZnO:PQX) arise from the high porosity of the sol-gel films.

X-ray diffraction analysis was performed to investigate the structural changes in ZnO:PQX composites upon thermal treatment. The XRD patterns of pure PQX powder and ZnO:PQX composite heated at 150°C and 300°C are presented in Fig. 7. The pure PQX powder exhibits characteristic diffraction peaks indicative of its crystalline structure. However, the ZnO:PQX composite heated at 150°C shows a dramatic reduction in diffraction peak intensity, suggesting a transition to an amorphous state or partial degradation of the organic component. For composites powders heated at 150°C, XRD analysis shows an almost complete disappearance of diffraction reflections, indicating loss of structural order due to amorphization or partial degradation. At 300°C, XRD data show only peaks corresponding to crystalline ZnO with wurtzite structure (JCPDS 36-1451), with no detectable reflections from the original PQX structure.

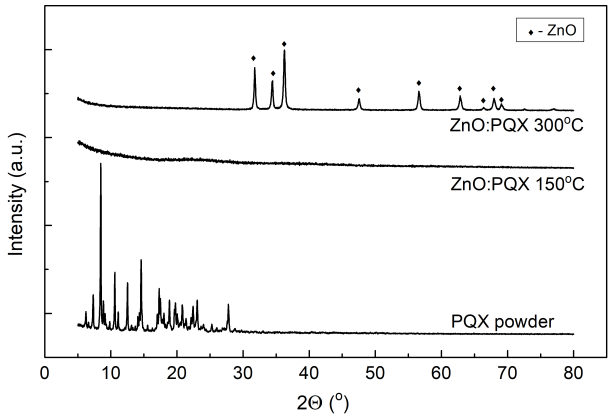

Fig. 7. X-ray diffraction patterns of three studied samples: PQX powder, ZnO:PQX heated at 150°C, and ZnO:PQX heated at 300°C

Thermal analysis of PQX powder presented in Fig. 8 reveals distinct thermal effects below 200°C, corresponding to structural reorganization without significant mass loss.

These observations align with ellipsometric data, which reveal thermal effects in thin films at temperatures as low as 100°C. Lower transformation temperatures in thin films compared to bulk powder arise from their higher surface-to-volume ratio, interfacial effects, and constrained geometry, all of which reduce activation energy for structural changes. The sol-gel processing environment and organic additives (DEA, TPSA) further increase thermal reactivity in thin films. Above 300°C, rapid thermal decomposition occurs, accompanied by significant mass loss between 300°C and 400°C due to bond breaking and volatile product release.

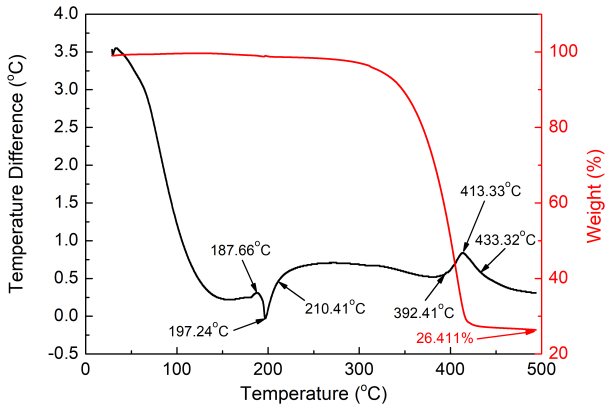

Fig. 8. Differential thermal analysis (DTA) and thermogravimetric analysis (TGA) of PQX powder

The surface morphology of ZnO and ZnO:PQX thin films on silicon substrates was characterized by AFM and SEM. AFM images are shown in Fig. 9.

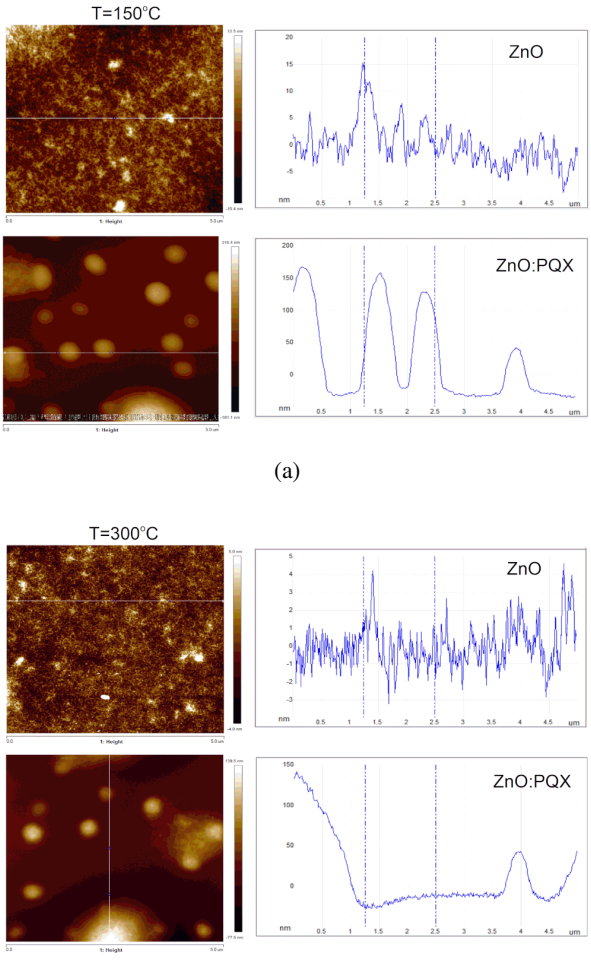

Fig. 9. AFM topography images and height profiles of ZnO and ZnO:PQX thin films annealed at: (a) 150°C, (b) 300°C

AFM images and the corresponding roughness profiles show that the ZnO film is smooth, with an RMS surface roughness (σRMS) of approximately 2.31 nm. The ZnO:PQX composite film exhibits a noticeably nonuniform surface, with a roughness of about 37.1 nm. After heating the samples for 1 h at 300°C, the roughness of both films decreases. The σRMS values are summarized in Table 3.

SEM images of selected ZnO and ZnO:PQX thin films annealed at different temperatures are shown in Fig. 10. On the surface of the ZnO layer, isolated grains are visible, which merge into larger, irregular aggregates on the surface of the ZnO:PQX composite layer. Individual grains of about 4 μm in size are observed on the surface of the ZnO film, whereas the surface of the ZnO:PQX film is rougher. Increasing the annealing temperature leads to the appearance of additional grains on both ZnO and ZnO:PQX surfaces, which is associated with the formation of the crystalline ZnO phase in the structure [12].

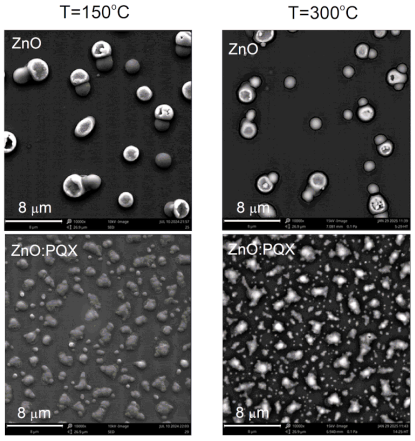

Fig. 10. SEM images of ZnO and ZnO:PQX thin films annealed at 150°C and 300°C

4. CONCLUSIONS

The paper presents the results of optical, thermo-optical, structural, and surface morphology studies of ZnO and ZnO:PQX composite thin films prepared by the sol-gel method using a spin-coating technique. The films were annealed at 150°C and 300°C.

Optical measurements show that the organic compound PQX in solution exhibits absorption in the blue region of the electromagnetic spectrum with simultaneous emission in the yellow–orange range, depending on solvent polarity. The largest Stokes shift was obtained in the most polar solvent (acetonitrile, Stokes shift 128 nm), which indicates the potential applicability of this dye as a luminophore in LSCs.

Thermo-optical studies in the temperature range 25–300°C showed that, during the first heating cycle, a significant decrease in the thickness of both the ZnO layer and the PQX-containing layer occurs. During cooling in the first cycle, as well as throughout the entire second heating–cooling cycle, both the film thickness and the refractive index are markedly more stable than during the initial heating step. This behavior may be associated with reorganization of the layer structure, release of residual gases, or changes in the surface morphology of the thin films. The determined TOC values are negative for both films. This may be because ZnO thin films prepared by the sol-gel method are porous and exhibit a relatively high TEC coefficient. Wide band gap materials such as ZnO have low electronic polarizability, which implies that the TOC coefficient is dominated by the volumetric thermal expansion coefficient, leading to a negative TOC value.

PQX exhibits limited thermal stability, with the onset of degradation already at 150°C and pronounced decomposition above 300°C. The annealing process leads to a transition from an ordered crystalline structure to an amorphous state, which accounts for the observed changes in optical properties. After complete PQX degradation at 300°C, only the pure ZnO phase with wurtzite structure remains, but with increased porosity, which explains the low refractive index values. The XRD results confirm that, after annealing above 300°C, the material can no longer be described as ZnO:PQX, but rather as porous ZnO containing residual organic fragments. SEM and AFM images show that the PQX-containing thin film is rougher and that, after annealing at 300°C, the roughness of both films decreases.

Based on these results, it can be concluded that, despite its favorable photophysical properties and large Stokes shift, the PQX dye has limited thermal stability, as evidenced by structural degradation beginning at 150°C. The incorporation of PQX into the ZnO matrix significantly reduces the refractive index (to approximately 1.1 for ZnO:PQX after heat treatment) and increases the surface roughness of ZnO:PQX thin films. This may lead to reduced photon absorption, lower emission, and decreased efficiency of potential LSC devices based on this composite material. Therefore, the results indicate that the ZnO:PQX composite system, in its present form, is not suitable for use in LSCs and requires further modification.

ACKNOWLEDGEMENTS

This research was partially funded by the National Science Centre, Poland, grant number: 2023/07/X/ST5/00214.

REFERENCES

[1] E. Muchuweni, T.S. Sathiaraj, and H. Nyakotyo, "Synthesis and characterization of zinc oxide thin films for optoelectronic applications," *Heliyon*, vol. 3, no. 4, p. e00285, Apr. 2017, doi: 10.1016/J.HELIYON.2017.E00285.

[2] P. Struk, T. Pustelny, K. Goaszewska, M.A. Borysiewicz, and A. Piotrowska, "Optical investigations of ZnO layers affected by some selected gases in the aspect of their application in optical gas sensors," *Bull. Pol. Acad. Sci. Tech. Sci.*, vol. 63, no. 4, pp. 829–836, 2015, doi: 10.1515/BPASTS-2015-0094.

[3] M. de J. Fimbres-Romero, A. Flores-Pacheco, M.E. Alvarez-Ramos, and R. Lopez-Delgado, "Transparent and Colorless Luminescent Solar Concentrators Based on ZnO Quantum Dots for Building-Integrated Photovoltaics," *ACS Omega*, vol. 9, no. 26, pp. 28008–28017, 2024, doi: 10.1021/acsomega.4c00772.

[4] S.I. Ibrahim, K.S. Rida, and B. Al-Ogaidi, "Effect of Thin Films of Rhodamine C Dye with Different Weights of ZnO

Nanoparticles on the Performance of Si-Solar Cell," *J. Eng. Appl. Sci.*, vol. 15, no. 13, pp. 2718–2722, 2020, doi: 10.36478/jeasci.2020.2718.2722.

[5] M. Khan *et al.*, "Investigation of Photoluminescence and Optoelectronics Properties of Transition Metal-Doped ZnO Thin Films," *Molecules*, vol. 28, no. 24, p. 7963, 2023, doi: 10.3390/molecules28247963.

[6] M. Atoui, S. Benzeghda, T. Touam, A. Chelouche, and D. Djouadi, "Ag Doping Effects on the Microstructure, Morphology, Optical, and Luminescence Properties of Sol–Gel-Deposited ZnO Thin Films," *Semiconductors*, vol. 55, no. 12, pp. 976–984, 2021, doi: 10.1134/S1063782621080030/METRICS.

[7] L.A. Zadorozhnaya, A.P. Tarasov, I.S. Volchkov, A.E. Muslimov, and V.M. Kanevsky, "Morphology and Luminescence of Flexible Free-Standing ZnO/Zn Composite Films Grown by Vapor Transport Synthesis," *Materials*, vol. 15, no. 22, p. 8165, 2022, doi: 10.3390/MA15228165.

[8] H. Guo *et al.*, "Self-Powered Luminescent Solar Concentrators-Integrated Temperature Detection System with High Thermal Tolerance by Reversible Thermal Photoluminescence Luminophores," *Adv. Funct. Mater.*, vol. 34, no. 49, p. 2409232, 2024, doi: 10.1002/ADFM.202409232.

[9] A.R. Hong, S. Shin, G. Kang, H. Ko, and H.S. Jang, "Intense Near-Infrared Light-Emitting NaYF4:Nd,Yb-Based Nanophosphors for Luminescent Solar Concentrators," *Materials*, vol. 16, no. 8, p. 3187, 2023, doi: 10.3390/MA16083187/S1.

[10] Z. Zhou *et al.*, "Enhanced Thermoelectric Performance of ZnO-Based Thin Films via Interface Engineering," *Crystals*, vol. 12, no. 10, p. 1351, 2022, doi: 10.3390/cryst12101351.

[11] O. Oluwaleye, B.W. Mwakikunga, and J.K.O. Asante, "Effects of Induced Structural Modification on Properties of V+ Ion-Implanted RF—Magnetron Sputtering Deposited ZnO Thin Films of Thickness 120 nm on Borosilicate Glass Substrates," *Nanomaterials*, vol. 15, no. 4, p. 278, 2025, doi: 10.3390/NANO15040278.

[12] V. Dalouji, "The incident photons cut-off energy, the optical linear equations and the electron phonon interactions in ZnO thin films annealed at different temperatures," *Heliyon*, vol. 10, no. 18, p. e37509, 2024, doi: 10.1016/J.HELIYON.2024.E37509.

[13] N. Nosidlak *et al.*, "The thermo-optical and optical properties of thin ZnO and AZO films produced using the atomic layer deposition technology," *J. Alloys Compd.*, vol. 900, p. 163313, 2022, doi: 10.1016/J.JALLCOM.2021.163313.

[14] A. Danel, K. Wojtasik, P. Szlachcic, M. Gryl, and K. Stadnicka, "A new regiospecific synthesis method of 1*H*-pyrazolo[3,4-*b*]quinoxalines – Potential materials for organic optoelectronic devices, and a revision of an old scheme," *Tetrahedron*, vol. 34, pp. 5072–5081, 2017, doi: 10.1016/j.tet.2017.06.061.

[15] P. Gąsiorski *et al.*, "Synthesis and spectral properties of halogen methyl-phenyl-pyrazoloquinoxaline fluorescence dyes: Experiment and DFT/TDDFT calculations," *J. Lumin.*, vol. 198, pp. 370–377, 2018, doi: 10.1016/j.optmat.2017.11.019.

[16] H. Fujiwara, *Spectroscopic Ellipsometry: Principles and Applications*; John Wiley & Sons Ltd.: Hoboken, NJ, USA, 2007.

[17] H.G. Tompkins and E.A. Irene, *Handbook of Ellipsometry*, William Andrew, Norwich, NY, USA, 2005.

[18] R.M.A. Azzam and N.M. Bashara, *Ellipsometry and Polarized Light*, North-Holland, Amsterdam, 1987.

[19] L. Prodhomme, "A new approach to the thermal change in the refractive index of glasses," *Phys. Chem. Glass.*, vol. 1, pp. 119–122, 1960.

[20] P. Gąsiorski *et al.*, "Synthesis and spectral properties of Methyl-Phenyl pyrazoloquinoxaline fluorescence emitters: Experiment and DFT/TDDFT calculations", *Opt. Mater.*, vol. 75, pp. 719–726, 2018, doi: 10.1016/j.optmat.2017.11.019.

[21] B. Johs, C.M. Herzinger, J.H. Dinan, A. Cornfeld, and J.D. Benson, "Development of a parametric optical constant model for $Hg_{1-x}Cd_xTe$ for control of composition by spectroscopic ellipsometry during MBE growth," *Thin Solid Films,* vol. 313–314 pp. 137–142, 1998, doi: 10.1016/S0040-6090(97)00800-6.

[22] J.A. Woollam, *CompleteEASE™Data Analysis Manual*, J.A. Woollam Co. Inc.: Lincoln, NE, USA, 2020.